crystals

MDPI

Article

Production of Nanocellulose Film from Abaca Fibers

Anniver Ryan Lapuz [1,2,†], Satoru Tsuchikawa [1], Tetsuya Inagaki [1], Te Ma [1] and Veronica Migo [3,*,†]

[1] Graduate School of Bioagricultural Sciences, Nagoya University, Aichi 464-8601, Japan; anniverryan.lapuz@fprdi.dost.gov.ph (A.R.L.); st3842@agr.nagoya-u.ac.jp (S.T.); inatetsu@agr.nagoya-u.ac.jp (T.I.); mate@agr.nagoya-u.ac.jp (T.M.)
[2] Department of Science and Technology Forest Products Research and Development Institute, Laguna 4031, Philippines
[3] Department of Chemical Engineering, University of the Philippines Los Baños, Luguna 4031, Philippines
* Correspondence: vpmigo@up.edu.ph
† These authors contributed equally to this work.

Abstract: Abaca fibers were subjected to a TEMPO mediated oxidation to extract nanocellulose on a 500 L capacity locally fabricated reactor. A yield of 46.7% white gel material with 2.23% solid content was obtained from an overnight reaction. Transmission electron microscopy scan of the white gel material confirms the production of relatively short highly individualized cellulose nanofibril (CNF) as the diameter of abaca fiber was reduced from 16.28 µm to 3.12 nm with fiber length in the range of 100 nm to 200 nm. Nanocellulose film was prepared using air drying (CNF-VC) and vacuum oven drying (CNF-OD). The effect of CNF concentration on the physical, morphological, thermal and mechanical properties were evaluated. FTIR spectra showed cellulose I spectra between abaca fiber with both the CNF-VC film and CNF-OD film with two distinct peaks at 1620 cm^{-1} and 1720 cm^{-1} attributed to the carboxyl group resulting from the TEMPO oxidation. In addition, the carboxyl group decreases in thermal stability of cellulose. Moreover, the XRD scan showed a decrease in crystallinity index of CNF films compared to abaca fibers. CNF-VC film showed the highest tensile strength at 0.4% concentration with 88.30 MPa, while a 89.72 MPa was observed for CNF-OD film at 0.8% concentration.

Keywords: nanocellulose; abaca; CNF; CNC; TEMPO; vapor casting; air-drying; vacuum oven drying; biofilm

check for updates

Citation: Lapuz, A.R.; Tsuchikawa, S.; Inagaki, T.; Ma, T.; Migo, V. Production of Nanocellulose Film from Abaca Fibers. *Crystals* **2022**, *12*, 601. https://doi.org/10.3390/cryst12050601

Academic Editors: Weiqian Tian, Liming Zhang and Sergejs Gaidukovs

Received: 23 March 2022
Accepted: 21 April 2022
Published: 25 April 2022

Publisher's Note: MDPI stays neutral with regard to jurisdictional claims in published maps and institutional affiliations.

Copyright: © 2022 by the authors. Licensee MDPI, Basel, Switzerland. This article is an open access article distributed under the terms and conditions of the Creative Commons Attribution (CC BY) license (https://creativecommons.org/licenses/by/4.0/).

1. Introduction

Nanocellulose has attracted various scientific and industrial communities for economic and environmental reasons with the goal of solving global climate change, resource shortages, and waste disposal [1–4]. Nanocellulose is essentially biodegradable, renewable, non-toxic, and sustainable carbohydrate-based polymer that can be used as a substitute for oil-based packaging material with comparable mechanical, rheological, and gas barrier properties [1,5,6]. Moreover, a large scale packaging solutions require highly transparent, flexible, and inexpensive high performance gas barrier materials. In addition, a low gas permeability as well as mechanical strength and flexibility are important target properties for laminates, coatings, and food packaging films [7].

Generally, cellulose nanocrystals (CNC) and cellulose nanofibrils (CNF) are the two main types of nanocellulose (NC) extracted from lignocellulosic material using top down approach. CNC also referred to as whiskers and rods are needle-like nanometrics having a fiber diameter within or less than 100 nm and fiber length to 5–2000 nm depending on the source of materials and hydrolysis conditions [8]. Traditionally, CNCs are obtained from fibers using strong acid to remove the amorphous region while retaining the more resistant crystalline region. On the other hand, CNF consists of an amorphous and crystalline region where aggregates of cellulose microfibrils have a fiber diameter in the range of 10–100 nm, while its length varies from 100 to several micrometers. It can be viewed as composed of

expanded high-volume cellulose, moderately degraded and greatly expanded in surface area, and obtained by a mechanical, biological, or chemical processes [9–11].

One of the methods used in extracting CNFs is the pretreatment of pulp fiber using 2,2,6,6,-tetramethylpiperidine-1-oxyl radical (TEMPO)-mediated system followed by very mild mechanical disintegration. Saito et al. [12] popularized the method of the oxidation pre-treatment method for hardwood pulp fibers using the TEMPO/NaBr/NaClO system at pH 10. Specifically, the TEMPO has been widely studied for catalytic and selective oxidation of primary hydroxyl groups under aqueous condition that significantly add a negatively charge at the surface that allow the repulsion of individual fibrils [13–17]. Isogai et al. [13] showed the relationship of reaction to the carboxylate content and degree of polymerization. As the reaction time is increased, the carboxylate and aldehyde content increased. However, the degree of polymerization decreased. Both types of nanocellulose possess a good gas barrier property, especially for oxygen because of the dense network structure that is formed by nanofibrils. In CNC, the density of the film can be attributed to the small and uniform particle sizes—whereas, for CNF, the densification is enhanced by the inherent flexibility of the wet material forming a denser film and sealing up the most spaces between the fibrils down to the molecular level. In contrast, CNC nanorods are inherently rigid and thus have a lower density of packing; therefore, a higher formation of pores is expected within the film [18].

Non-wood plant materials have gained increasing attention as a source of nanomaterials compared to wood due to its availability, owing to its shorter maturity period. Among the non-wood plant materials, abaca fiber seems to be an attractive source of nanocellulose due to its high cellulose content [11,19]. Chemically, abaca fiber is composed of cellulose (66.43%), hemicellulose (24.7%), lignin (13.6%), and low water content (0.7%) responsible for its high mechanical strength [20,21]. Abaca is an endemic plant of the Philippines and is in the family of Musacea (banana). Therefore, the country is also the top exporter of abaca fibers with about 85% share of the world's imports, while the remaining 15% of the supply is mostly accounted for by Ecuador [22]. In 2020, the volume of abaca produced was approximately 423,699.10 in bales, which is around 74% of the total fiber produced in the country [23]. Traditionally, abaca fibers are used as cordage and in handicrafts while processed fibers or abaca pulp are used for paper and specialty paper products [21–24]. Recently, Alila et al. [11] have studied the potential use of abaca fiber to extracted nanocellulose using TEMPO mediated oxidation followed by mild disintegration. The extracted nanocellulose showed a fiber diameter around 20 nm and with relatively short lengths that possess a higher fraction of individualized thin fibrils. With the current laws and restriction on the use on oil-based plastic in the country, abaca seems to be the ideal candidate as a viable economical source of nanocellulose. Thus, this study evaluates the large scale production of nanocellulose from abaca fiber using a locally fabricated 500 L reactor as an initial step toward a productive capacity. The physical, morphological, chemical, thermal, and mechanical properties vapor cast films were also evaluated.

2. Materials and Methods

2.1. Materials

Commercial bleached abaca pulp with alpha cellulose of 87.34% was obtained from Albay Agro-Industrial Development Corporation (ALINDECO, Albay, Philippines). Hydrochloric acid (37%) and 2,2,6,6-tetramethylpiperidine-1-oxyl (TEMPO) (98%) were of analytical grade. Sodium bicarbonate (99.62%), sodium carbonate (99.80%), sodium bromide (99.0%), potassium chloride (98.22%), sodium hypochlorite (8.28%), and sodium chlorite (80%) were technical grade and were purchased from a local trader. All chemicals were used without further purification.

2.2. Pretreatment of Abaca Fiber

Abaca fiber slurry with a consistency of 2% was mixed with 2 wt% of sodium chlorite at pH 2 using a potassium chloride hydrochloric acid buffer solution. The slurry was stirred overnight to increase further the alpha cellulose. Afterwards, the slurry was washed and the pretreated pulp was collected. The pretreated pulp was never dried and had a solid content of 14.32% to enhance disintegration and fibrillation during nanocellulose extraction.

2.3. Nanocellulose Extraction

A 500 L capacity locally fabricated reactor was used for the large scale production of nanocellulose. The never dried pretreated abaca fibers with alpha cellulose content of 90.20% (TAPPI T-203 cm-09) were disintegrated in a sodium carbonate-bicarbonate buffer solution set at pH 10. Sodium bromide (1.0%), TEMPO (0.16%) and sodium hypochlorite (23 mol/kg) were added and continuously stirred. The reaction was allowed to proceed overnight until a cloudy solution was observed.

2.4. Production of Nanocellulose Film

Nanocellulose film was produced using a vapor casting technique. CNF suspension with 0.2%, 0.4%, 0.6%, 0.8%, and 1.0% concentration were homogenized (rpm = 5000) for 10 min to obtain a uniform CNF distribution. Afterwards, the suspension was poured into a plastic mold and placed in a vacuum oven (CNF-OD) set at 50 °C until dry. Additionally, another batch with the same CNF concentration was air-dried (CNF-VC) under room temperature.

2.5. Scanning Electron Microscopy

Morphological analysis of abaca fiber and CNF films was done using electron microscopy. Abaca fiber and CNF films were precoated with platinum particles using an MC1000 Ion Sputter Coater (Hitachi, Ibaraki, Japan) before being subjected to a scanning electron microscope (FEI Inspect S50, Eidenhoven, The Netherlands) operated at 12.50 kV with 500× magnification. On the other hand, dilute suspension of CNF was dropped on a Cu-grid and allowed to stand for 10 min. A 5% of uranyl acetate was used to stain the grit and dried in a HUS-5 Hitachi High Vacuum. Afterwards, the sample was placed in a desiccating oven overnight. A transmission electron microscope (JEOL TEM-1220, Tokyo, Japan) operated at 80 kV with 30,000× magnification was used to determine the nanocellulose morphology. Fiber morphology was measured using ImageJ® 1.52a.

2.6. FTIR Spectroscopy

The infrared spectra of cellulose were obtained using Fourier Transform Infrared Spectrophotometer (Shimadzu IR Prestige 21, Shimadzu, Kyoto, Japan) equipped with a Single Reflection Diamond Attenuated Total Reflectance (ATR) accessory. Samples were clamped with constant pressure to ensure a good optical contact with ATR diamond. The spectra were taken in the range of 650 cm^{-1}–4000 cm^{-1} at a resolution of 4 cm^{-1} with a total of 45 scans for each sample. FTIR assures that the process of nanocellulose extraction was successfully conducted since all the expected functional groups have been identified at their specific peaks.

2.7. Thermal Analysis

Thermal properties of abaca fiber and CNF films were characterized using Differential Scanning Calorimetry (DSC Q500, TA Instruments, New Castle, DE, USA). Abaca fiber and representative samples for both casting methods were analyzed at the temperature range of 30 °C to 500 °C using a heating rate of 10 °C/min under a nitrogen environment.

2.8. X-ray Diffraction (XRD) Analysis

Abaca fiber and representative CNF film of CNF-VC and CNF-OD were subjected to an X-ray equatorial diffraction profiles using a X-ray Diffraction (Shimadzu XRD-6100, Shimadzu, Kyoto, Japan) equipped with a Cu target with wavelength of 1.54060 angstrom, operating voltage and current of 40 kV and 30 mA, respectively. The diffraction intensities were recorded between 2° and 60° (2θ) angles. The crystallinity index (CI) was measured using a Segal's method (1):

$$CI = \frac{I_{200} - I_{\text{am}}}{I_{200}} \quad (1)$$

where I_{200} is the crystallinity region (2θ = 22.6°) and I_{am} is the amorphous region (2θ = 18.0°).

2.9. Physical and Mechanical Properties of CNF Film

The physical properties of the CNF films were evaluated using a thickness tester (PTI Frank, Hessen, Germany) and an analytical balance for its thickness and weight, respectively. The tensile strength of CNF film was determined following an ASTM D882-25598 Standard Test Method for Tensile Properties of Thin Plastic Sheeting. Three replicates were prepared and five test samples measuring 10 mm × 100 mm were prepared per replicate. The samples were conditioned at 23 °C and RH 50% for 1 week prior to testing. A single column universal testing machine (UTM) (Instron 4444, Norwood, MA, USA) set at a crosshead speed of 5 mm/min with a grip gap of 50 mm was used to determine the tensile strength of the CNF films.

3. Results and Discussion

3.1. Nanocellulose Extraction

A white gel like material with a solid content of 2.23% was collected after washing and filtered at the bottom half of the reactor (Figure 1). The gel like material appearance corresponds to the high hygroscopic property of nanocellulose. The yield was recorded at 46.70%, which is within the range of 40–70% yield as reported by Alila et al. [11].

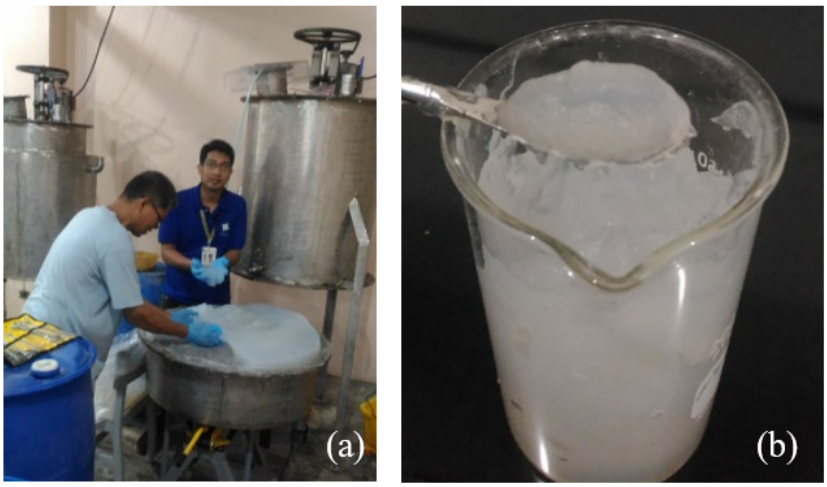

Figure 1. Large scale production of NC-TEMPO (**a**) collection of CNF-TEMPO; (**b**) gel like CNF-TEMPO slurry.

3.2. Scanning Electron Microscopy (SEM)

The effect of TEMPO oxidation of abaca fibers was observed using scanning electron microscopy. Initially, abaca fibers had a diameter of around 16.28 µm as shown in Figure 2a. A comparable finding was observed from Alila et al. [11] and Waller et al. [22], where the fiber diameters are within 3–30 µm. However, after the TEMPO oxidation of abaca fibers, the extracted CNF has a relatively short and highly individualized fiber with an average diameter of 3.12 nm and in a range of 100 nm to 200 nm fiber length.

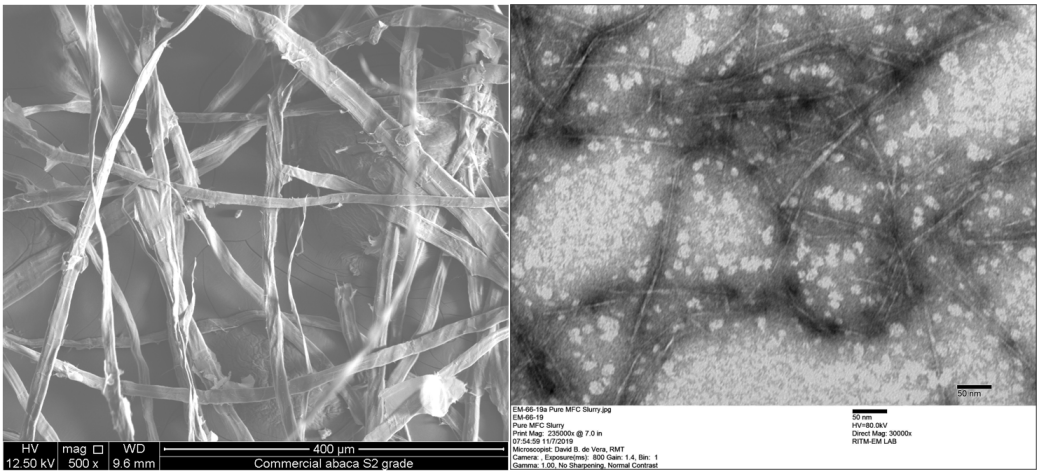

Figure 2. Extraction of nanocellulose (**a**) abaca fiber and (**b**) nanocellulose.

Similar results were reported by Alila et al. [11], wherein TEMPO oxidation of abaca fiber followed by mild homogenization obtained nanocellulose with relatively short fiber length with a range of 200 nm up to 1 µm and fiber diameter around 20 nm. Moreover, the abaca fibrils exhibit less aptitude to form an entangled network, and their interaction seems to occur through lateral interaction. In comparison, hemp, jute, and flax extracted from stalks show thicker fibrils within 30–50 nm in range and relatively long fibrils with lengths exceeding several microns with difficulty in determining the extremities. All are in an interwoven web like structure. It can be seen that fibers from leaves seem to release thinner and shorter fibrils than those extracted from stalks that exhibited a greater tendency to form a highly entangled network. The pretreatment of abaca fibers coupled with TEMPO oxidation at a high oxidant level and prolonged reaction time provide enough conditions for the production of relatively short highly individualized CNF.

Figure 3 shows the effect of CNF concentration on the morphology of CNF films for both air dried and vacuum oven drying. As the concentration of CNF is increased from 0.2% to 1.0%, the surface of the film appears smooth but gradually changed into being thick with a rough texture owing to the cellulose and agglomeration and intercalation of among the nanofibers [25–27].

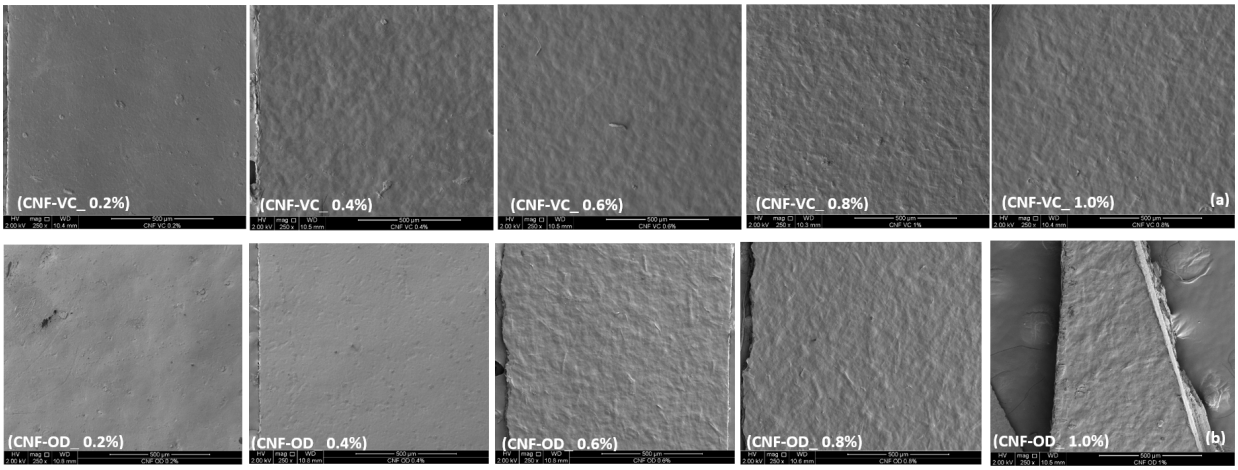

Figure 3. Effect of CNF concentration on surface morphology of (**a**) CNF-VC and (**b**) CNF-OD.

The surface morphology of the films can provide additional information that can support the physical and mechanical properties of nanocellulose film.

3.3. FTIR Spectroscopy

The FTIR spectra of abaca fiber and representative sample for both CNF-VC film and CNF-OD film are shown in Figure 4. Typically, cellulose molecules have a high amount of OH bonds for hydroxyl group and CH bonds specifically present around 3300 cm^{-1} and 2900 cm^{-1} for the hydrocarbon group [6,20].

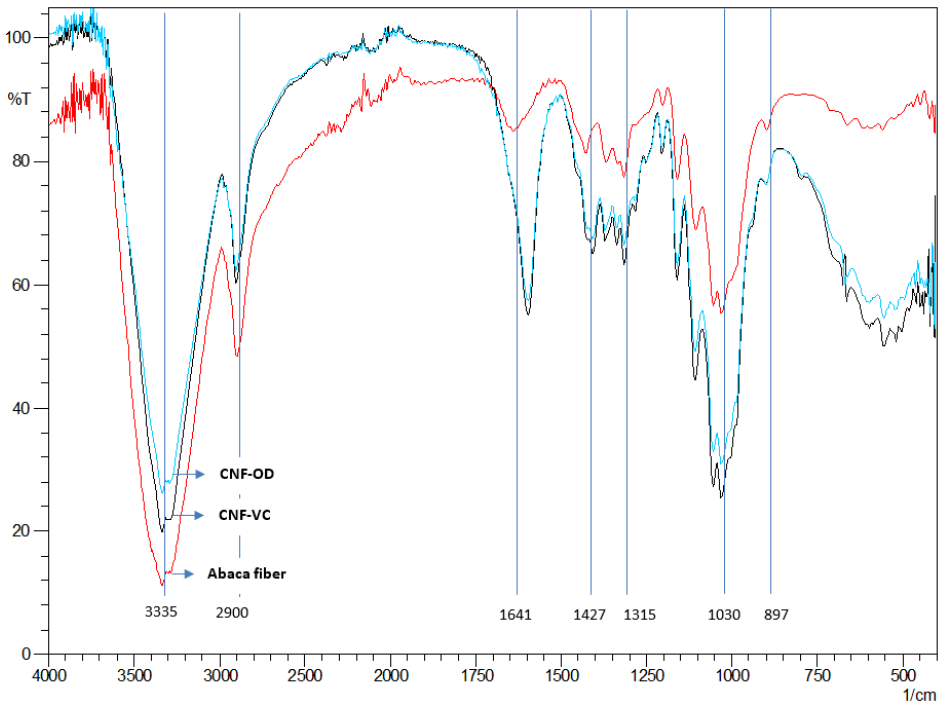

Figure 4. FTIR spectra of abaca fiber and CNF films.

The absorption bands around 1427 cm^{-1}, 1315 cm^{-1}, and 1029 cm^{-1} correspond to the scissoring, stretching, bending vibrations of -CH_2, -CH, -OH, and C-O bonds in cellulose. The crystalline structure of the cellulose is also observed in the peak at around 1420 cm^{-1} while the amorphous region is located at around 890 cm^{-1} [28]. The major difference between the spectra is in the peaks at 1590 cm^{-1} of resultant CNF films are attributed to carboxylate groups. The peak around 1650 cm^{-1} from the abaca fiber is attributed to the residual lignin [16]. In addition, a lower light small absorption at 1720 cm^{-1} indicates the C=O groups in the protonated carboxyl groups, which was not present from the abaca fiber. These differences indicate the addition of the carboxylate group on the cellulose surface as a result of the TEMPO oxidation [6].

3.4. Thermal Analysis

DSC thermographs of abaca fiber and a representative sample of CNF-VC film and CNF-OD film is presented in Figure 5. The broad endothermic peak observed at around 40–160 °C for all the samples represent the heat of vaporization of the absorbed moisture due to hydrophilic hydroxyl surfaces on cellulose that attract and retain moisture [29].

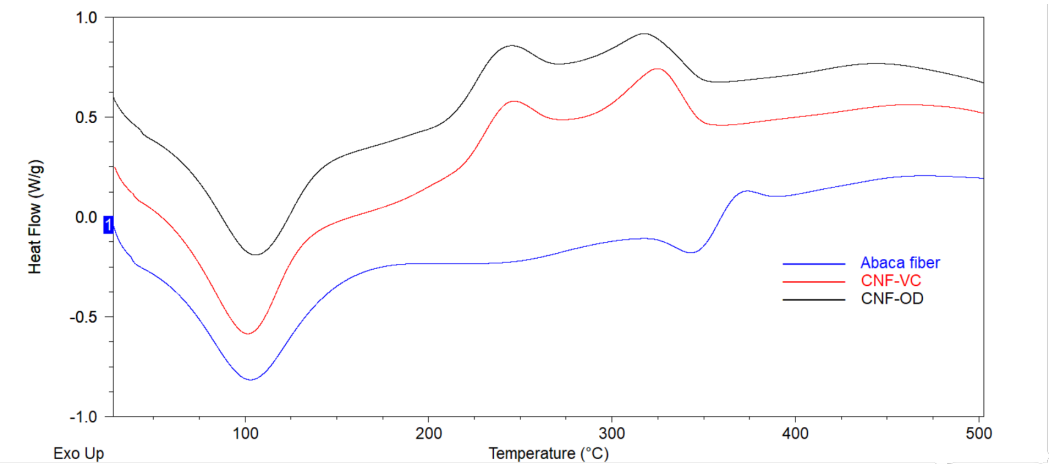

Figure 5. DSC scans of cellulose materials.

The occurrence of exothermic peak for both CNF films at 244 °C and 330 °C corresponds to the decomposition of amorphous and crystalline region of nanocellulose, respectively, which is lower to the decomposition temperature of abaca fiber, which occurred at 368 °C [30]. The lowering of the decomposition temperature and thermal stability for both films can be attributed to the attached carboxylate group and lower molecular weight or degree of polymerization of cellulose after the TEMPO oxidation. In addition, a secondary endothermic peak for abaca fiber at 346 °C can be attributed to the course of fusion or melting process that resulted in the decomposition of cellulose [6,20,29–31]. Compared to CNF films, the abaca fiber rendered more compact crystal structure after raw abaca fiber was chemically pretreatment where the non-cellulosic materials was removed and cellulose crystals undergo reorientation process. Thus, the decomposiiton temperature of abaca fiber occured at a higher temperature around 368 °C [29].

3.5. X-ray Diffraction Analysis

The diffraction pattern of CNF-VC film and CNF-OD film compared to abaca fiber is presented in Figure 6. Based on the results, CNF films showed a similar diffraction pattern as the cellulose I structure of abaca native cellulose fiber with diffraction peaks at 2θ = 14°(101) and 22° (002) confirming the retaining of the original structure of cellulose after the TEMPO oxidation. These results indicate that the carboxylate groups formed by TEMPO-mediated oxidation are selectively present on cellulose microfibril surfaces without any internal cellulose crystallites [13].

However, the CI of CNF-VC film and CNF-OD film slightly decreased compared to abaca fibers from 64.48% to 59.89% and 58.11%, respectively. The slight decrease in CI can be attributed to prolonged TEMPO oxidation that incorporated carboxylate on the surface of cellulose, which caused a reduction of expose cellulose crystal [6,29,31]. Furthermore, the presence of inter-molecular and intra-molecular hydrogen linkage between a crystalline zone of fibers only allows the selective surface oxidation of cellulose crystals, while the inner part of crystals remains intact, reducing the exposure of the crystalline domain accessible for further oxidation [29]. The narrowing of crystal structure of nanocellulose film compared to abaca fiber was evident in the reduction of d-spacing of abaca fibers from 3.96 nm to 3.93 nm and 3.92 nm for CNF-OD film and CNF-VC film, respectively.

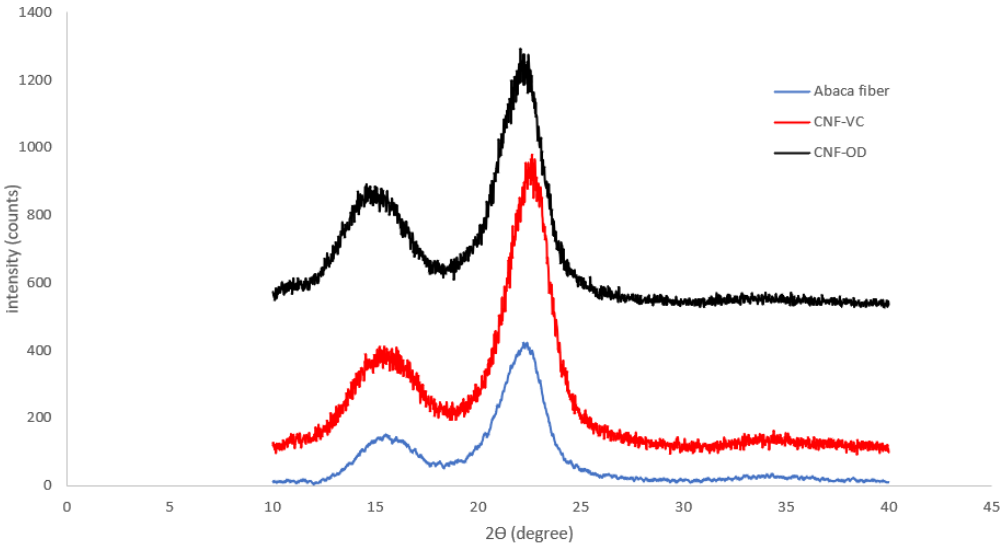

Figure 6. XRD scans of cellulose materials.

3.6. Physical and Mechanical Properties of CNF Films

The effect of CNF concentration on the physical properties of CNF-VC film and CNF-OD film is summarized in Tables 1 and 2, respectively. Generally, the weight, thickness, and grammage for both the CNF-VC film and CNF-OD film increased as the concentration of CNF is increased. The density of CNF-VC film seems to plateau after the initial concentration and decreases at 1.0%. However, the density of CNF-OD film seems to be more uniform as compared to CNF-VC film, probably due to a more controlled condition.

Table 1. Physical properties of CNF-VC film at different CNF concentrations.

CNF %	Weight (g)	Thickness (mm)	Basis Weight (g/m^2)	Density (g/cm^3)
0.2%	0.0058	0.0028	28.93	1.031
0.4%	0.0112	0.0047	56.00	1.195
0.6%	0.0113	0.0051	56.43	1.141
0.8%	0.0243	0.0103	121.17	1.182
1.0%	0.0335	0.0168	177.53	1.061

Table 2. Physical properties of CNF-OD films at different CNF concentrations.

CNF %	Weight (g)	Thickness (mm)	Basis Weight (g/m^2)	Density (g/cm^3)
0.2%	0.0030	0.0020	14.97	0.784
0.4%	0.0048	0.0027	23.97	0.861
0.6%	0.0091	0.0047	45.47	0.968
0.8%	0.0119	0.0097	59.37	0.961
1.0%	0.0224	0.0120	111.90	0.944

The mechanical property of nanocellulose film depends mainly on the single fiber mechanical property and interfiber bonding [32]. Interfiber bonding can be facilitated by homogeneous dispersion, higher packaging density, and more overlapping between neighboring fibers [33]. Figure 7 shows the tensile strength of CNF-VC film and CNF-OD film.

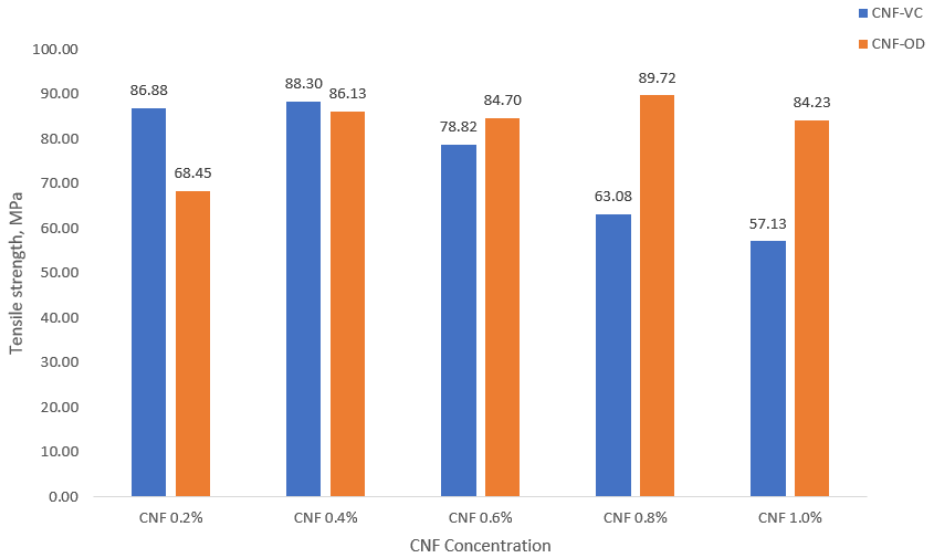

Figure 7. Tensile strength of CNF films.

Generally, a decrease in tensile strength was observed as the concentration of CNF was increased for CNF-VC film. In contrast, an increase in tensile strength of CNF-OD film was observed as CNF concentration was increased. As mentioned earlier, mechanical properties are dependent on interfiber bonding. High density would indicate a compact packing of CNF film, which indicates good interfiber bonding. Moreover, smooth surface film morphology would indicate a good fiber dispersion essential also for good interfiber bonding. However, less dense CNF film with highly rough surface morphology would imply weak interfiber bonding due to low contact among fibers due to fiber aggregation [33–35]. A maximum tensile strength of 88.30 MPa for CNF-VC film was observed at 0.4% CNF with 1.195 g/cm^3, whereas a maximum tensile strength of 89.72 MPa was observed at 0.8% CNF with 0.961 g/cm^3 for CNF-OD film. However, 0.8% CNF seems to have a rougher surface morphology compared to 0.4% CNF; perhaps, it presents the overlapping or networking among fibers, which may have caused its higher tensile strength [33,35].

Compared to the results of Fukuzumi et al. [36], CNF films prepared from 200 nm fiber length showed a tensile strength of 224 MPa. The 2.5× higher tensile strength is influenced by the different fiber source and the uniformity of CNF materials. These factors will account for the individual fiber strength and interfacial fiber bonding, respectively.

4. Summary and Conclusions

Nanocellulose was successfully extracted using TEMPO oxidation of abaca fiber at a large scale as an initial step for the establishment of a productive capacity. A white gel material was produced with 2.23% solid content. TEM scan confirmed the extraction of relatively short individualized CNF with fiber diameter of 3.12 nm and with over 100 nm in fiber length. Subsequently, CNF film was successfully prepared using air drying and vacuum oven drying. FTIR, DSC, and XRD analyses have shown that the chemical, thermal, and crystallographic properties of the CNF film have slightly been altered due to the addition of carboxyl group. The weight, thickness, and grammage of CNF films generally increased as the concentration of CNF was increased. The maximum tensile strength for CNF-VC film and CNF-OD film was observed at 0.4% (w/v) with 88.30 MPa and at 0.8% (w/v) with 89.72 MPa, respectively. Lastly, the tensile properties of CNF film showed the potential use of abaca nanomaterial as a substitute for oil-based packaging material.

Author Contributions: All the authors worked all together for the conceptualization of the project. Regular meetings were supervised by S.T. to evaluate the progress of the project. Investigation of the project was mostly conducted by A.R.L. and V.M. Draft preparation was primarily written by A.R.L., S.T., V.M., I.T. and T.M. reviewed and edited the manuscript. All authors have read and agreed to the published version of the manuscript.

Funding: The author would like to acknowledge the support of Department of Science and Technology—Forest Products Research and Development Institute.

Institutional Review Board Statement: Not applicable.

Informed Consent Statement: Not applicable.

Data Availability Statement: Not applicable.

Acknowledgments: We are grateful to Mario Ramos for the SEM analysis of CNC films. We also thank Rebecca Lapuz and Kim Balagot for the FTIR analysis of the samples.

Conflicts of Interest: The authors declare no conflict of interest.

References

1. Fotie, G.; Limbo, S.; Piergiovanni, T. Manufacturing of food packaging based on nanocellulose: Current advances and challenges. *Nanomaterials* **2020**, *10*, 1726. [CrossRef] [PubMed]
2. Li, S.; Lee, P. Development and applications of transparent conductive nanocellulose paper. *Sci. Technol. Adv. Mater* **2017**, *62*, 621. [CrossRef] [PubMed]
3. Li, M.C.; Wu, Q.; Moon, R.; Hubbe, M.; Bortner, M. Rheological aspects of cellulose nanomaterials: Governing factors and emerging applications. *Adv. Mater.* **2021**, *33*, 2006052. [CrossRef]
4. Dai,H.; Ou, S.; Huang, Y.; Huang, H. Utilization of pineapple peel for production of nanocellulose and film application. *Cellulose* **2018**, *25*, 1743–1756. [CrossRef]
5. Zheng, D.; Zang, Y.; Guo, Y.; Yue, J. Isolation and characterization of nanocellulose with a novel shape from walnut (*Juglans regia* L.). *Polymers* **2019**, *11*, 1130. [CrossRef] [PubMed]
6. Hastuti, N.; Kanomata, K.; Kitaoka, T. Characteristics of TEMPO-oxidized cellulose nanofibers from oil palm empty fruit bunches produced by different amounts of oxidant. *Conf. Ser. Earth Environ. Sci.* **2019**, *359*, 012008. [CrossRef]
7. Aulin, C.; Lindstrom, T. Cellulose nanofibril films and coatings for packaging applicatpion. In *Production and Applications of Cellulose Nanomaterials*; Postek, A., Moon, R., Rudie, A., Bilodeau, M., Eds.; Tappi Press: Peachetree Corners, GA, USA, 2013; pp. 229–231.
8. Moon, R.; Beck, S.; Rudie, A. Cellulose nanocrystal-Material with unique properties and many potential applications. In *Production and Applications of Cellulose Nanomaterials*; Postek, A., Moon, R., Rudie, A., Bilodeau, M., Eds.; Tappi Press: Peachetree Corners, GA, USA, 2013; pp. 9–12.
9. Perumal, A.B.; Nambiar, R.B.; Moses, J.A.; Anandharamakrishnan, C. Nanocellulose: Recent trends and applications in food industry. *Food Hydrocoll.* **2022**, *127*, 107484. [CrossRef]
10. Isogai, A. Emerging nanocellulose technologies: Recent developments. *Adv. Mater.* **2020**, *33*, 2000630. [CrossRef]
11. Alila, S.; Besbes, I.; Vilar, M.; Mutje, P.; Boufi, S. Non-woody plants as raw materials for production of microfibrillated cellulose (MFC): A Comparative Study. *Ind. Crop. Prod.* **2013**, *41*, 250–259. [CrossRef]
12. Saito, T.; Kimura, S.; Nishiyama, Y.; Isogai, A. Cellulose nanofibers prepared by TEMPO-mediated oxidation of native cellulose. *Biomacromolecules* **2007**, *8*, 2485–2491. [CrossRef] [PubMed]
13. Isogai, A.; Saito, T.; Fukuzumi, H. TEMPO-oxidized cellulose nanofibrils. *Nanoscale* **2011**, *3*, 71. [CrossRef] [PubMed]
14. Reiner R.; Rudie, A. Pilot plant scale-up of TEMPO-pretreated cellulose nanofibrils. In *Production and Applications of Cellulose Nanomaterials*; Postek, A., Moon, R., Rudie, A., Bilodeau, M., Eds.; Tappi Press: Peachetree Corners, GA, USA, 2013; pp. 177–178.
15. Besbes, I.; Alila, S.; Boufi, S. Nanofibrillated cellulose from TEMPO-oxidized eucalyptus fibers: Effect of the carboxyl content. *Carbohydr. Polym.* **2011**, *84*, 975–983. [CrossRef]
16. Jatiño-Masó, J.; Serra-Parareda, F.; Tarrés, Q.; Mutjé, P.; Espinach, F.; Delgado-Aguilar, M. TEMPO-oxidized cellulose nanofibers: A potential bio-Based superabsorbent for diaper production. *Nanomaterials* **2019**, *9*, 1271. [CrossRef] [PubMed]
17. Abraham, E.; Deepa, B.; Pothan, L.; Jacob, M.; Thomas, S.; Cvelbar, U.; Anandjiwala, R. Extraction of nanocellulose fibrils from lignocellulosic fibres: A novel approach. *Carbohydr. Polym.* **2011**, *86*, 1468–1475. [CrossRef]
18. Ferrer, A.; Pal, L.; Hubbe, M. Nanocellulose in packaging: Advances in barrier layer technologies. *Ind. Crop. Prod.* **2017**, *95*, 574–582. [CrossRef]
19. Jawaid, M.; Abdul Khalil, H. Cellulosic/synthetic fibre reinforced polymer hybrid composites: A review. *Carbohydr. Polym.* **2011**, *86*, 1–18. [CrossRef]
20. Saragih, S.; Lubis, R.; Wirjosentono, B.; Eddyanto. Characteristic of abaca (Musa textilis) fiber from Aceh Timur as bioplastic. In *The 3rd International Seminar on Chemistry*; AIP Publishing: New York, NY, USA, 2018; p. 2049.

21. Moreno, L.; Protacio, C.M. Chemical composition and pulp properties of Abaca (Musa textilis Nee) cv. Inosa harvested at different stages of stalk maturity. *Ann. Trop. Res.* **2012**, *34*, 45–62.
22. Abaca in the Philippines: An Overview of a Potential Important Resource for the Country. Available online: https://kth.diva-portal.org/smash/get/diva2:1352495/FULLTEXT01.pdf (accessed on 21 October 2021).
23. Philippine Fiber Industry Development Authority. Fiber Statistics 2020. Available online: http://www.philfida.da.gov.ph/index.php/2016-11-10-03-32-59/2016-11-11-07-56-39/fiber-statistics-2020 (accessed on 3 February 2021).
24. Abaca. Available online: https://www.fao.org/economic/futurefibres/fibres/abaca0/en/ (accessed on 21 October 2021).
25. Tonoli, G.; Teixeira, E.; Corrêa, A.; Marconcini, J.; Caixeta, L.; Pereira-da-Silva, M.; Mattoso, L. Cellulose micro/nanofibres from Eucalyptus kraft pulp: Preparation and properties. *Carbohydr. Polym.* **2012**, *89*, 80–88. [CrossRef]
26. Suryanto H.; Sutrisno, T.; Yanuhar, U.; Wulandari, R. Morphology and structure of bacterial cellulose film after ionic liquid treatment. *J. Phys.* **2020**, *1595*, 012028. [CrossRef]
27. Johar, N.; Ahmad, I. Morphological, thermal, and mechanical properties of starch biocomposite films reinforced by cellulose nanocrystals from rice husks. *BioResources* **2012**, *7*, 5469–5477. [CrossRef]
28. Hospodarova, V.; Singovszka, E.; Stevulova, N. Characterization of cellulosic fibers by FTIR spectroscopy for their further implementation to building materials. *Am. J. Anal. Chem.* **2018**, *9*, 303–310. [CrossRef]
29. Hassan, S.; Velayutham, T.; Chen, Y.; Lee, H. TEMPO-oxidized nanocellulose films derived from coconut residues: Physicochemical, mechanical and electrical properties. *Int. J. Biol. Macromol.* **2021**, *180*, 392–402 [CrossRef] [PubMed]
30. Miao, X.; Lin, J.; Bian, F. Utilization of discarded crop straw to produce nanofibrils and their assemblies. *J. Bioresour. Bioprod.* **2020**, *5*, 26–36. [CrossRef]
31. Fukuzumi, H.; Saito, T.; Okita, Y.; Isogai, A. Thermal stabilization of TEMPO-oxidized cellulose. *Polym. Degrad. Stab.* **2010**, *95*, 1502–1508 [CrossRef]
32. Wang, W.; Sabo, R.; Mozuch, M.; Kersten, P.; Zhu, J.Y.; Jin, Y. Physical and mechanical properties of cellulose nanofibril films from bleached eucalyptus pulp by endoglucanase treatment and microfluidization. *J. Polym. Environ.* **2015**, *23*, 551–558. [CrossRef]
33. Barbash, V.; Sapkota, B.; Rangari, V. Eco-friendly cellulose nanofiber extraction from sugarcane bagasse and film fabrication. *Sustainability* **2020**, *12*, 6015. [CrossRef]
34. Meng, Q.; Wang, T. Mechanics of Strong and Tough Cellulose Nanopaper. *Appl. Mech. Rev.* **2019**, *71*, 040801. [CrossRef]
35. Henriksson, M.; Berglund, L.; Isaksson, P.; Lindstro, T.; Nishino, T. Cellulose Nanopaper Structures of High Toughness. *Biomacromolecules* **2008**, *9*, 1579–1585. [CrossRef] [PubMed]
36. Fukuzumi, H.; Saito, T.; Isogai, A. Influence of TEMPO-oxidized cellulose nanofibril length on film properties. *Carbohydr. Polym.* **2013**, *93*, 172–177. [CrossRef] [PubMed]